Size dependence of the coalescence and melting of iron clusters: A molecular-dynamics study

Feng Ding,[1,2,*] Arne Rosén,[1] and Kim Bolton[1]
[1]*Experimental Physics, School of Physics and Engineering Physics, Göteborg University and Chalmers University of Technology, SE-412 96, Göteborg, Sweden*
[2]*Department of Physics, Qufu Normal University, Qufu 273165, Shandong, People's Republic of China*
(Received 26 February 2004; revised manuscript received 11 June 2004; published 31 August 2004)

Molecular-dynamics simulations show that the coalescence of iron nanoclusters ($Fe_N + Fe_N \rightarrow Fe_{2N}$, where up to $2N = 10\,000$ atoms, or a diameter of 6 nm, has been studied) occurs at the temperatures lower than the cluster melting point, and that the difference between coalescence and melting temperatures increases with decreasing cluster size. Thus, the temperature at which small metal nanoclusters are observed to coalescence, e.g., in the experimental growth of carbon nanotubes, is not the same as their melting point.

DOI: 10.1103/PhysRevB.70.075416 PACS number(s): 61.46.+w, 36.40.−c

I. INTRODUCTION

A. Catalyst clusters in carbon nanotube growth

Transition metal clusters, such as iron, nickel, cobalt and their alloys, are often used as catalysts in the production of carbon nanotubes (CNTs).[1,2] For example, in chemical vapor deposition (CVD) growth, iron can be introduced as a thin layer of metal iron on a suitable substrate. At the elevated temperatures necessary for CNT growth (800–1500 K), the layer of deposited iron forms Fe clusters, which catalyze nanotube growth. The size of the clusters that, together with other parameters such as the temperature and pressure, determine the diameter and quality of the nanotubes, can be controlled by varying the thickness of the deposited iron layers.[3]

The catalyzed CNT growth mechanism is not fully understood. The vapor-liquid-solid (VLS) model,[4–7] where the metal cluster acts as both a catalyst and a solvent, is the most widely accepted growth model. When acting as a catalyst, the metal cluster decomposes carbon feedstock (e.g., methane or carbon monoxide) to release carbon atoms, and these atoms can then dissolve in the metal solvent to form metal carbide. According to the model, once the liquid metal-carbide cluster is supersaturated in carbon, and the cluster begins to cool, carbon atoms precipitate from the particle and form CNTs.

It was initially proposed,[7] and is still widely believed, that the metal-carbide cluster needs to be in the liquid state to allow for rapid diffusion of carbon atoms within the metal cluster before they precipitate to form CNTs. Although the melting points of bulk Fe (1809 K), Co (1768 K) and Ni (1726 K) are far higher than the temperature used in CVD production of CNTs (about 800 K–1500 K), it is known that the melting point of small clusters is lower than that of corresponding bulk.[8,9] Furthermore, the melting point of metal-carbide alloys is lower than the melting point of the pure metal. For example, the eutectic points of Fe–C, Co–C, and Ni–C are 1421, 1594, and 1602 K, respectively, which are more than 100 K lower than the melting points of the pure metals. However, recent experimental results of catalyzed carbon nanofiber growth (5–20 nm Ni particles at 500–800 K)[10] indicate that the particles are in the solid state during nanofiber growth and the growth occurs from step defects on the cluster surface. Even though the cluster appears to be in the solid state, there is extensive deformation of the cluster during fiber growth.

B. Melting of metal nanoclusters

Theoretical studies[11,12] predict that the decrease in metal cluster melting point is proportional to the inverse of the cluster diameter. This relationship has been validated experimentally[13–17] and by computer simulations,[9,18] and Table I lists the relationship between the cluster, T_m, and bulk, T_{bulk}, melting points for some 5 and 10 nm metal and metal-carbide clusters. All species show larger deviations from the bulk melting point with decreasing cluster size, and these deviations are less than 10% for the 10 nm clusters and 20% for the 5 nm clusters. The results for the Fe and FeC clusters, which were obtained from simulations,[9] show that the melting point of a 10 nm cluster is just 4–5% lower than the bulk melting point, which is in agreement with the experimental observations that 30 nm Fe (or FeC) cluster particles are solid during carbon nanofiber growth (which, as mentioned above, occurs at ≈500–800 K).[10]

In CVD experiments the size of the catalyst cluster is typically between 1 and 100 nm, and the temperature is between 800 and 1500 K.[19,20] The data in Table I thus indicate

TABLE I. The relative melting points of some 5 and 10 nm metal and metal-carbide clusters. T_m and T_{bulk} are the cluster and bulk melting points, respectively.

Material	5 nm $(T_{\text{bulk}} - T_m / T_{\text{bulk}})$	10 nm $(T_{\text{bulk}} - T_m / T_{\text{bulk}})$	Reference
Au	0.18	0.08	13
Al	0.08	0.04	14
Ni	0.15	0.07	18
Pb	0.12	0.06	15
Sn	0.20	0.10	16
Ag	0.02	0.01	17
Fe	0.10	0.05	9
$Fe_{90\%}C_{10\%}$	0.09	0.04	9

that large Fe and FeC clusters will be solid, at least under low temperature growth conditions. For example, according to the data in the table the 10 nm cluster has a 1350 K melting point, and larger clusters will have even higher melting points. On the other hand, the inverse diameter dependence of the cluster melting point mentioned above yields melting points of 1 nm clusters of about 700–800 K, and these small clusters will be molten at CVD growth temperatures. (Previous simulations show that the melting points of these small clusters can be affected by magic number geometries which removes the ideal inverse diameter dependence. Nonetheless, the melting points of these clusters are scattered around the value predicted by the simple diameter dependence.[9])

C. Coalescence of metal nanoclusters

Indirect evidence of metal and metal-carbide cluster melting may also be obtained from experiments that analyze the change in cluster shape under CNT growth conditions. These include the observations that (i) the catalyst is often prepared as a deposited metal layer and, upon heating to CNT growth temperatures, the layer forms metal clusters.[3] This shape transition of the layer to cluster structure is taken as evidence of melting and that the clusters are in the liquid phase. (ii) Catalyst metal particles can be encapsulated in CNTs as short rodlike structures.[21] The mechanism that leads to these structures, which is thought to involve the adsorption of the liquid metal drop into the nanotube, implies that the cluster is liquid. (iii) Catalyst clusters that are found on the CNT ends after the growth process often have a trinodal shape.[6] Since this is different to the initial shape of the cluster (which is often a sphere or hemisphere), it is taken as evidence for the liquid state of the cluster during growth. (iv) Most recently, and of particular relevance to the present work, studies of Fe, FeC, Co, and CoC clusters show that two or more clusters between 10 and 30 nm in diameter can coalesce into one large spherical or elongated (rodlike) cluster.[22] The coalescence is taken as evidence for melting and the coalescence temperature is assumed to be the melting point. It was thereby found that 30 nm Fe, FeC, Co, and CoC clusters melt at the temperature about 40–50% lower than the corresponding bulk melting or eutectic point. This is in stark contrast to the results discussed above (where 10 nm cluster melting points were just 10% below the bulk melting point—see Table I), as well as the experimental observation of solid phase 5–20 nm catalyst particles during carbon nanofiber growth.[10]

The correlation between the change in catalyst particle shape at elevated temperatures and its melting point is based on the assumption that change in cluster shape, or the coalescence of small clusters, within the experimental time requires rapid diffusion of cluster atoms (on the surface and/or in the bulk) which can only be obtained in the liquid phase. In this contribution we use molecular dynamics (MD) to study the relationship between Fe cluster coalescence and melting and, in particular, to determine if change in cluster shape through coalescence requires the clusters to be in the liquid phase. It is found that Fe clusters can coalescence at the temperatures below their melting points, with the deviation in coalescence and melting temperatures increasing with decreasing cluster size.

II. POTENTIAL ENERGY SURFACE AND SIMULATION METHODS

Previous investigations have shown that the many-body interaction potential, which is based on the second moment approximation of the tight binding model,[23,24] is good for studying the thermal properties of the pure[25–28] and alloy[29] transition metal systems. The interaction energy between iron atoms can be written as a sum of Born-Mayer-type repulsive energies and many-body attractive energies as

$$E = \sum_{i \neq j} A \exp\left[-p\left(\frac{r_{ij}}{r_0} - 1 \right) \right] - \left\{ \sum_{i \neq j} \xi^2 \exp\left[-2q\left(\frac{r_{ij}}{r_0} - 1 \right) \right] \right\}^{1/2},$$

where r_{ij} is the distance between the ith and jth iron atoms. The parameters $A=0.133\,15$ eV, $\xi=1.6179$ eV, $p=10.50, q=2.60$, and $r_0=2.553$ Å—taken from Ref. 29—are obtained by fitting the cohesive energy, lattice parameter and elastic constants of γ-Fe (fcc structure) to experimental data. Although this potential energy surface is fit to data for bulk Fe, simulations show that it also reproduces correct trends for Fe clusters. For example, as discussed with reference to Fig. 3, the simulated cluster melting point shows the correct (inverse diameter) dependence on the cluster size. In addition, in agreement with experiment,[30] simulations based on this potential show that the fcc structure dominates for large ($N>2000$) clusters whereas many smaller clusters have icosahedral or decahedral symmetries. Simulations based on this potential are thus expected to give valid data for the cluster dynamics discussed in this work, and simulations of other metal clusters[25–28] (e.g., Au, Ag, Ni) have also been based on this type of potential energy surface.

The coalescence of $Fe_N + Fe_N \rightarrow Fe_{2N}$, where N ranged from 150 to 5000 atoms were simulated (i.e., cluster diameters were between $\approx$1.5 and 6 nm). As discussed below, the Fe_N clusters were initially at low temperatures, even after impact with each other, and the temperature was subsequently raised to induce coalescence. The initial low temperature crystalline Fe_N structures were obtained as follows: The N Fe atoms were randomly placed in a spherical box and relaxed to a local energy minimum using a steepest descent method (this was done to prevent the cluster from exploding when two atoms were initially too close to each other). The cluster was subsequently heated to 2000 K, which is well above the melting point (all cluster melting points are below the bulk melting point of 1800 K). The crystalline structure was then obtained from simulated annealing[31] of the 2000 K structure, where the temperature for $(i+1)$st annealing cycle is $T_{i+1}=0.95T_i$ and 50 000 trajectory steps (150 ps) were propagated for each temperature cycle. The trajectory step was 3 fs and the temperature was controlled by the Berendsen scaling method.[32] The annealing was terminated once the temperature was between 100 and 400 K (lower tempera-

tures were required for smaller clusters) and the final crystalline structure was obtained from the annealed structure using the steepest decent method. Although this structure is probably not the global minimum energy structure, it is expected to be very similar to the minimum energy structure, and previous simulations of cluster thermal properties have shown that they are not sensitive to small variations in the initial structure.[9]

Two crystalline Fe_N clusters, that were separated by $D+0.4$ nm, where D is the diameter of the FeN cluster, were used to initiate the coalescence simulations. The closest distance between any two atoms belonging to different clusters was thus ≈ 0.4 nm and, although the attractive force between the clusters was weak, it was sufficient to lead to impact of the clusters. The trajectory of this initial impact, which contained 200 000 time steps, was done at a very low temperature to prevent cluster coalescence and melting (e.g., 400 K was used for $Fe_{5000}+Fe_{5000} \rightarrow Fe_{10000}$). This Fe_N-Fe_N collision complex was then heated by increasing its temperature in cycles of 20 K, where 200 000 trajectory steps were performed for each temperature cycle.

The coalescence process was analyzed by monitoring the exchange of atoms between the Fe_N clusters, as well as the change in shape of the Fe_{2N} cluster. In the case of the Fe_{2N} cluster, the average distance between the Fe atoms and the cluster center of mass (i.e., the radius of gyration[33]) is

$$D_{\text{ave}} = \frac{1}{2N}\sum_{i=1}^{2N} |\vec{r}_i - \vec{r}_C|,$$

where $\vec{r}_i$ is the position of the ith atom and $\vec{r}_C$ is the center of mass. The temperature dependence of this quantity was obtained by calculating D_{ave} at the final step of each temperature cycle. D_{ave} is sensitive to the shape of the Fe_{2N} cluster, having a maximum value when the two Fe_N clusters are separated and decreasing when the clusters coalesce. A minimum value for D_{ave} is obtained for spherical Fe_{2N} clusters, which is the shape of the liquid clusters (and is also the shape of some solid phase clusters at temperatures just below the melting point).

The cluster melting point is determined by monitoring the change in cluster energy as a function of temperature [and is discussed with reference to Fig. 2(b) below]. A sharp rise in energy over a small temperature change indicates the solid $\rightarrow$ liquid phase transition and, similar to previous work,[18] the melting point is defined as the temperature at which the phase transition ends. We note that the melting point of a Fe_{2N} cluster does not depend on whether the initial conditions of the cluster are obtained from the impact of two Fe_N clusters, as discussed above, or if the Fe_{2N} cluster is initially in its crystalline geometry. The data reported here (Fig. 3) are obtained from both types of initial conditions.

Defining a coalescence temperature, T_c, is more difficult than defining the melting point, since coalescence is associated with a change in cluster shape and not (necessarily) a phase change. For consistency with the experiments described above, the clusters are considered to have coalesced once a rodlike structure is formed (these structures, see structure in Fig. 1(C), are similar to the elongated coalesced structures seen experimentally[22]). Experimental measurements are not able to identify which atoms originate from each of the Fe_N clusters after coalescence to these rodlike structures (in simulations the atoms that belong to the initial clusters can be tracked). The simulations reveal that the large Fe_{2N} clusters have formed rodlike structures when D_{ave} differs by less than 10% from its minimum value, and thus the coalescence temperature, T_c, is defined as the temperature when D_{ave} is 10% above its minimum value (as discussed above, the minimum value of D_{ave} occurs when the cluster is molten). Although this choice of T_c is somewhat arbitrary, its exact value does not affect the results presented here.

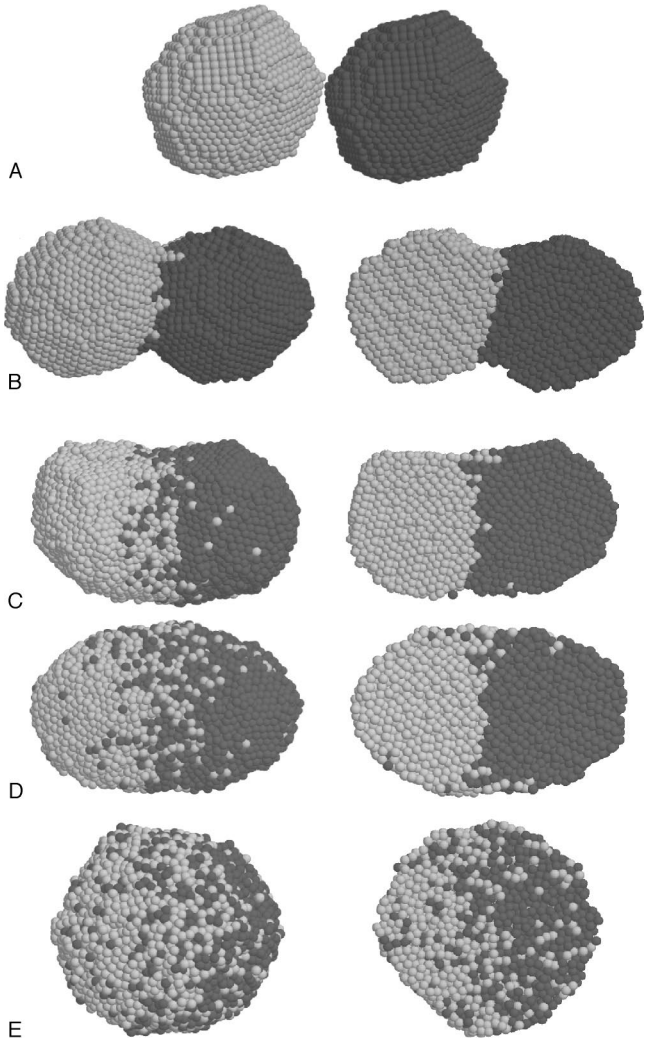

FIG. 1. Snapshots at different temperatures during $Fe_{5000}+Fe_{5000} \rightarrow Fe_{10000}$ coalescence and melting. Structures A (initial structure at 400 K), B (800 K), C (1200 K), D (1400 K), and E (1460 K). The left pictures in B–E are of the entire cluster and show the surface atoms, whereas the pictures on the right-hand side are cross sections through the clusters.

III. RESULTS AND DISCUSSION

Typical structures during $Fe_{5000}+Fe_{5000} \rightarrow Fe_{10000}$ coalescence and melting are shown in Fig. 1. The pictures on the

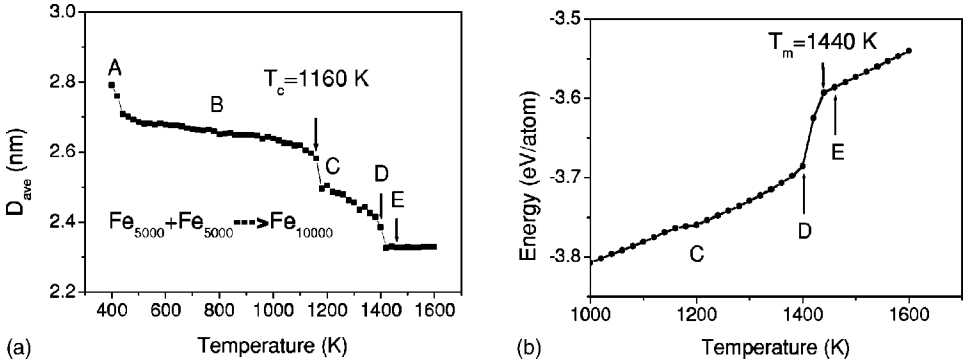

FIG. 2. Temperature dependence of D_{ave} (a) and cluster energy (b) during the $Fe_{5000}+Fe_{5000} \rightarrow Fe_{10000}$ coalescence and melting. Points A–E correspond to the structures shown in Fig. 1.

left-hand side are snapshots of the entire cluster and show the surface atoms, whereas the pictures on the right-hand side are cross sections through the clusters. Structure A in Fig. 1 shows the initial conditions where the Fe_{5000} crystalline clusters are at 400 K. Upon impact the atoms near the interface between the two clusters reorganize because of their new local environment (which has changed from vacuum to other Fe atoms), and a peanut shaped cluster similar to that shown in B of Fig. 1 is formed. This peanut structure is found at all temperatures from the point of impact until complete coalescence to the rodlike structure seen in C of Fig. 2, although the separate shapes of the initial Fe_{5000} clusters (that are seen in structure B in Fig. 1 for the structure at 800 K) become less discernable with increasing temperature. It is also clear from the figure that, for this peanut structure, there is very little exchange of surface or bulk atoms between the two initial Fe_{5000} clusters, and the clusters have a crystalline structure. When the temperature is increased to 1200 K there is extensive diffusion of surface atoms which leads to a rodlike structure and coalescence (C in Fig. 2). Although the surface atoms are sufficiently mobile to allow for coalescence and exchange of atoms between the two Fe_{5000} clusters, there is extremely little exchange of bulk atoms [see the cross-sectional picture in C of Fig. 1] that is associated with atomic diffusion in the liquid phase. Thus, as has been reported previously,[34–36] coalescence results from rapid surface diffusion of atoms from unstable high curvature regions to more stable low curvature regions. From an atomistic perspective, atoms that have low coordination (i.e., fewer neighboring atoms at the vortices and edges in high curvature regions) diffuse to regions where they have the largest coordination. The negative curvature of the neck region of the Fe_{10000} peanut-shaped cluster makes this the most stable region on the surface, and atoms diffuse to the neck to form the rodlike structure. As is discussed below, the temperature where the rodlike structure is formed (i.e., the coalescence temperature) which is $\approx$1200 K in the simulations, depends on the simulation (annealing) time. Longer simulation times will enable the rodlike structure to form at lower temperatures, which will yield lower coalescence temperatures.

As discussed above, the coalescence and melting temperatures are obtained from the temperature dependence of D_{ave} and cluster energy, respectively, and are shown in Fig. 2 for $Fe_{5000}+Fe_{5000} \rightarrow Fe_{10000}$. Although the entire temperature range of this simulation is shown in Fig. 2(a), only a limited interval is shown in Fig. 2(b) for the sake of clarity. The structures shown in Fig. 1 were obtained at the temperatures marked A–E in Fig. 2. As can be seen by the sharp increase in the cluster energy in Fig. 2(b), the melting point for the Fe_{10000} cluster is 1440 K. This temperature, which marks the onset of rapid diffusion of bulk atoms seen between D and E in Fig. 1, is higher than the temperature required for coalescence to the rodlike structure C in Fig. 1. In fact, as seen in Fig. 2(a), the definition of T_c given above yields a coalescence temperature of 1160 K, slightly below the temperature of the structure C shown in Fig. 1 (1200 K). It should also be noted that the coalescence temperature is well below the melting point of Fe_{5000}, which is 1400 K.

It is interesting to note that the coalescence (or change in shape) of the cluster below the melting point is not always smooth. This can be seen, for example, by the abrupt decrease in D_{ave} at C in Fig. 2(a). These sudden changes in D_{ave} do not appear in all the trajectories studied, and they can appear at any temperature between the initial and coalescence temperatures. Preliminary analysis indicates that the presence and temperature of this decrease depends on the initial cluster structure, and may be due to a metastable structure that abruptly relaxes to a more stable geometry once a sufficiently high temperature has been reached (these sudden decreases in D_{ave} should be less prevalent for longer simulations when the metastable structures have longer times to relax). The abrupt change in cluster shape is accompanied by a decrease in the rate of change in the cohesive energy [see C in Fig. 2(b)], which is consistent with a restructuring of the cluster geometry.

Figure 3 shows the cluster size dependence of the coales-

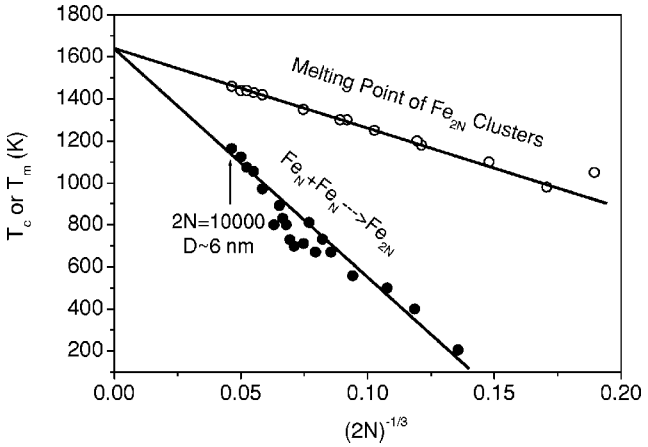

FIG. 3. Size dependence of $Fe_N+Fe_N \rightarrow Fe_{2N}$ coalescence temperatures (solid circles) and Fe_{2N} melting points (open circles).

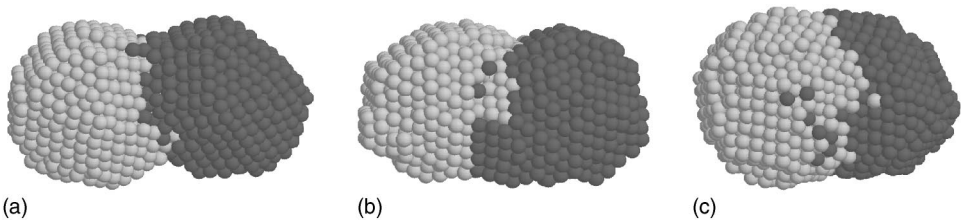

FIG. 4. Structures obtained during the $Fe_{1000}+Fe_{1000}\rightarrow Fe_{2000}$ coalescence when the temperature is 800 K. The structure in (a) is obtained when 0.15 ns trajectories are run for each temperature cycle during the simulation, (b) for 0.60 ns trajectories, and (c) for 2.4 ns trajectories.

cence and melting temperatures. As discussed above, in agreement with previous theoretical predictions and experimental observations[11–17] the melting point decreases linearly with the inverse of the cluster diameter [i.e., it decreases linearly with $(2N)^{-1/3}$ for a Fe_{2N} cluster]. The discrepancy between the bulk melting point extrapolated from the simulations (1640 K) and the experimental value (1809 K) was also observed in studies of Ni clusters,[18] and was explained as arising from the free surface effects of the clusters. However, inaccuracies in the PES may also contribute to this deviation. Figure 3 also shows that, apart from the slope, the coalescence temperature has a similar linear dependence on the cluster diameter [i.e., also $(2N)^{-1/3}$]. This may be due to the fact that, as discussed above, the cluster surface curvature, which is proportional to the inverse of the diameter, is the driving force for the coalescence process. Hence, similarly to the melting of nanoparticles[11–13,15] where curvature effects also play a dominant role, the change in coalescence temperature will also have an inverse diameter dependence. It is also clear from Fig. 3 that the difference in coalescence and melting temperatures increases for smaller clusters. This is because smaller clusters have larger curvature and, as discussed above, it is the curvature effects that give rise to the surface diffusion needed for cluster coalescence. Similarly, it is evident that the coalescence and melting temperatures converge for bulk materials, which agrees with the fact that two bulk materials cannot coalesce unless they are molten (since here there are no large curvature effects that gave rise to the surface diffusion needed for cluster coalescence).

As discussed with reference to Fig. 1, the calculated coalescence temperature depends on the simulation time since longer trajectories will allow for surface diffusion to form the rodlike structure at lower temperatures. That is, longer simulation times will yield lower coalescence temperatures, which will increase the difference between the coalescence and melting temperatures shown in Fig. 3. This is illustrated in Fig. 4 for $Fe_{1000}+Fe_{1000}\rightarrow Fe_{2000}$ coalescence, where all three structures are for the Fe_{2000} cluster at 800 K, but the structures in panels (a)–(c) are obtained when 0.15, 0.60, and 2.4 ns trajectories are propagated for each temperature cycle, respectively. It is clear that the structure in panel (a) has a well-defined peanut shape and thus the coalescence is not complete, that the initial Fe_{1000} cluster structures are still discernable in panel (b) [but not to the same extent as in panel (a)], and that the structure in panel (c) is rodlike. Thus, short simulation times yield a coalescence temperature larger than 800 K, whereas longer simulations predict lower coalescence temperatures. Experimental times are many orders of magnitude longer than the simulation times used here. This provides a possible explanation for the experimental observation that the coalescence temperature of a 30 nm Fe (or Co) cluster is about 40–50% lower than the bulk melting point,[22] whereas the coalescence of a 30 nm Fe cluster extrapolated from the data in Fig. 3 is just 5–6% lower than the bulk melting point.

IV. CONCLUSION

MD simulations of the $Fe_N+Fe_N\rightarrow Fe_{2N}$ coalescence and melting of iron clusters show that both the coalescence and melting temperatures decrease linearly with decreasing cluster diameter, that coalescence occurs at temperatures lower than the melting point, and that the difference in coalescence and melting temperatures increases for smaller clusters. Furthermore, the simulations show that lower coalescence temperatures are obtained when longer integration times are used for the annealing, which indicates that coalescence occurs at much lower temperatures under typical experimental conditions (where annealing can occur over seconds or longer).

In contrast to coalescence of bulk materials, curvature effects are important during coalescence of clusters. In general, the smaller the cluster the larger the surface curvature and the larger the diffusion rates of surface atoms. Since the surface diffusion dominates the coalescence process (i.e., cluster coalescence can occur without the diffusion of bulk atoms), it can occur without the clusters being molten. Hence, experimental observation of catalyst metal clusters changing shape is not sufficient evidence that the cluster is in the liquid state. As discussed with respect to the catalyzed growth of carbon nanofibers,[10] the high surface diffusion rates of metal and carbon atoms on the cluster surface may be sufficient to catalyze the growth of carbon nanostructures.

ACKNOWLEDGMENTS

The authors are grateful for the time allocated on the Swedish National Supercomputing facilities and for financial support from the Swedish Research Council and the Swedish Foundation for Strategic Research (CARAMEL consortium).

*Author to whom correspondence should be addressed. Electronic address: fengding@fy.chalmers.se

[1] *Carbon Nanotubes: Synthesis, Structure, Properties and Application*, edited by M. S. Dresselhaus, G. Dresselhaus, and Ph. Avouris (Springer, Berlin, 2001).
[2] H. Dai, Surf. Sci. **500**, 218 (2002).
[3] J. I. Sohn, C.-J. Choi, S. Lee, and T.-Y. Seong, Jpn. J. Appl. Phys., Part 1 **41**, 4731 (2002).
[4] T. Nozaki, Y. Kimura, and K. Okazaki, J. Phys. D **35**, 2779 (2002).
[5] J. Gavillet, A. Loiseau, C. Journet, F. Willaime, F. Ducastelle, and J.-C. Charlier, Phys. Rev. Lett. **87**, 275504 (2001).
[6] G. Y. Zhang, X. C. Ma, D. Y. Zhong, and E. G. Wanga, J. Appl. Phys. **91**, 9324 (2002).
[7] R. T. K. Baker, M. A. Barber, P. S. Harris, F. S. Feates, and R. J. Waite, J. Catal. **26**, 51 (1972).
[8] A. Rytkonen, H. Häkkinena, and M. Manninen, Eur. Phys. J. D **9**, 451 (1999).
[9] F. Ding, K. Bolton, and A. Rosén, J. Vac. Sci. Technol. A **22**, 1471 (2004).
[10] S. Helveg, C. López-Cartes, J. Sehested, P. L. Hansen, B. S. Clausen, J. R. Rostrup-Nielsen, F. Abild-Pedersen, and J. K. Nørskov, Nature (London) **427**, 426 (2004).
[11] R. R. Vanfleet and J. M. Mochel, Surf. Sci. **341**, 40 (1995).
[12] H. Reiss, P. Mirabel, and R. L. Wetten, J. Phys. Chem. **92**, 7241 (1988).
[13] P. A. Buffat and J. P. Borel, Phys. Rev. A **13**, 2287 (1976).
[14] S. L. Lai, J. R. A. Carlsson, and L. H. Allen, Appl. Phys. Lett. **72**, 1098 (1998).
[15] K. F. Peters, J. B. Cohen, and Y. W. Chung, Phys. Rev. B **57**, 13 430 (1998).
[16] S. L. Lai, J. Y. Guo, V. Petrova, G. Ramanath, and L. H. Allen, Phys. Rev. Lett. **77**, 99 (1996).
[17] M. Dippel, A. Maier, V. Gimple, H. Wider, W. E. Evenson, R. L. Rasera, and G. Schatz, Phys. Rev. Lett. **87**, 095505 (2001).
[18] Y. Qi, T. Cagin, W. L. Johnson, and W. A. Goddard, J. Chem. Phys. **115**, 385 (2001).
[19] S. Maruyama, R. Kojima, Y. Miyauchi, S. Chiashi, and M. Kohno, Chem. Phys. Lett. **360**, 229 (2002).
[20] H. Dai, A. G. Rinzler, P. Nikolaev, A. Thess, D. T. Colbert, and R. E. Smalley, Chem. Phys. Lett. **260**, 471 (1996).
[21] C. J. Lee, J. Park, S. Han, and J. Ihm, Chem. Phys. Lett. **337**, 398 (2001).
[22] Y. Homma *et al.*, J. Phys. Chem. B **107**, 12161 (2003).
[23] V. Rosato, M. Guillope, and B. Legrand, Philos. Mag. A **59**, 321 (1989).
[24] R. P. Gupta, Phys. Rev. B **23**, 6265 (1981).
[25] A. Posada-Amarillas and I. L. Garzón, Phys. Rev. B **54**, 10 362 (1996).
[26] I. L. Garzón and A. Posada-Amarillas, Phys. Rev. B **54**, 11 796 (1996).
[27] I. L. Garzón, K. Michaelian, M. R. Beltrán, A. Posada-Amarillas, P. Ordejón, E. Artacho, D. Sánchez-Portal, and J. M. Soler, Phys. Rev. Lett. **81**, 1600 (1998).
[28] K. Michaelian, N. Rendón, and I. L. Garzón, Phys. Rev. B **60**, 2000 (1999).
[29] J. Stanek, G. Marest, H. Jaffrezic, and H. Binczycka, Phys. Rev. B **52**, 8414 (1995).
[30] O. Kitakami, H. Sato, Y. Shimada, F. Sato, and M. Tanaka, Phys. Rev. B **56**, 13 849 (1997).
[31] S. Kirkpatrick, C. D. Gelatt, Jr., and M. P. Vecchi, Science **220**, 671 (1983).
[32] H. J. C. Berendsen, J. P. M. Postma, W. F. van Gunsteren, A. DiNola, and J. R. Haak, J. Chem. Phys. **81**, 3684 (1984).
[33] L. J. Lewis, P. Jensen, and J.-L. Barrat, Phys. Rev. B **56**, 2248 (1997).
[34] C. R. Stoldt, A. M. Cadilhe, C. J. Jenks, J.-M. Wen, J. W. Evans, and P. A. Thiel, Phys. Rev. Lett. **81**, 2950 (1998).
[35] A. Bogicevic, S. Liu, J. Jacobsen, B. Lundqvist, and H. Metiu, Phys. Rev. B **57**, R9459 (1998).
[36] P. Jensen, N. Larralde, J. L. Barrat, C. Misbah, and A. Pimpinelli, Eur. Phys. J. B **11**, 497 (1999).